Atmospheric Blocking in an Aquaplanet and the Impact of Orography

Veeshan Narinesingh[1,2], James F. Booth[1,2], Spencer K. Clark[3], Yi Ming[4]

[1]Department of Physics, City University of New York – The Graduate Center, New York, New York, 10016, United States of America

[2]Department of Earth and Atmospheric Sciences and NOAA-CESSRST, City University of New York – City College, New York, New York, 10031, United States of America

[3]Program in Atmospheric and Oceanic Sciences, Princeton University, Princeton, New Jersey, 08544, United States of America

4 Atmospheric Physics Division, NOAA Geophysical Fluid Dynamics Laboratory, Princeton, New Jersey, 08540, United States of America

Correspondence to: Veeshan Narinesingh (veenarinesingh@gmail.com)

Abstract.

This work utilizes an idealized moist GCM to investigate atmospheric blocking in terms of dynamics, spatial frequency, and duration. The model is first configured as an aquaplanet, then orography is added in separate integrations. Block-centered composites of wave activity fluxes and height show that blocks in the aquaplanet undergo a realistic dynamical evolution when compared to reanalysis. Blocks in the aquaplanet are also found to have similar lifecycles to blocks in model integrations with orography. These results affirm the usefulness of both zonally symmetric and asymmetric idealized model configurations for studying blocking. Adding orography to the model leads to an increase in blocking. This mirrors what is observed when comparing the northern (NH) and southern hemispheres (SH) of Earth, where the NH contains more orography, and thus more blocking. As the prescribed mountain height is increased, so does the magnitude and size of climatological stationary waves, resulting in more blocking overall. Increases in blocking however, are not spatially uniform. Orography is found to induce regions of enhanced block frequency just upstream of mountains, near high pressure anomalies in the stationary waves which is poleward of climatological minima in upper level zonal wind. While block frequency minima and jet maxima occur eastward of the wave trough. This result matches what is observed near the Rocky Mountains. Finally, an analysis of block duration shows blocks generated near stationary wave maxima last slightly longer than blocks that form far from, or without orography.

1 Introduction

Atmospheric blocks are quasi-stationary anticyclones that can cause temperature extremes (Sillman et al., 2011; Pfahl and Wernli, 2012), steer hurricanes and extratropical cyclones (Mattingly et al., 2015; Booth et al. 2017, respectively), and induce persistent weather (Cassou et al., 2005; Dole et al., 2011; Brunner et al., 2018). Despite the expensive and sometimes deadly impacts of blocks, many fundamental questions remain regarding their behaviour, and models tend to underpredict blocks in terms of their frequency and duration (D'andrea et al., 1998; Matsueda, 2009). As such, this paper utilizes an idealized general circulation model to expand our understanding of blocks, focusing on the representation in models configured with and without mountains.

Some have argued that blocks are consequences of an interaction between eddies and stationary waves induced by orography (Egger, 1978; Charney and Devore, 1979; Tung and Lindzen, 1979; Luo, 2005). These studies suggest mountains are critical for the overall existence of blocking and setting the location of climatological block frequency maxima. On the other hand, Shutts (1983) used a barotropic model to show that blocking flows do not necessarily need stationary forcing and can arise purely through interactions between transient eddies. Confirming this, Hu et al. (2008), Hassanzadeh et al. (2014), and Nabizadeh et al. (2019) have more recently shown that blocks do indeed occur in idealized models in the absence of zonally asymmetric forcing.

This suggests the extratropical cyclones (i.e., synoptic-scale eddies) that occur upstream of the blocking regions may be key. Colucci (1985) and Pfahl et al. (2015) show that extratropical cyclones can impact blocks downstream of the storm track exit region. In a related theory, blocks are linked to Rossby wave-breaking (Pelly and Hoskins, 2003; Berrisford et al., 2007; Masato et al., 2012), which primarily occurs in regions of weak westerly flow.

Hu. et al. (2008) presents case studies that show blocks in an aquaplanet model behave in a realistic manner. They also find that blocks in their aquaplanet model occur more frequently than what is observed in nature – regardless of hemisphere, which is contradictory to the idea that stationary waves facilitate blocking episodes. The results of Hu et al. (2008) however, are complicated by known discrepancies within the community regarding the identification (e.g. Barnes et al., 2012) and seasonality (Barriopedro et al., 2010) of blocking. In Hu et al. (2008), results from their perpetual equinox aquaplanet are compared to Weidenmann et al. (2002), who use a different block identification algorithm on reanalysis over all seasons. Thus, questions remain regarding the relative frequency of blocks with and without the presence of mountains.

The climatological spatial distribution of blocks is well documented. In the cool months of the Northern Hemisphere (NH), two main regions of blocking occur at the north-eastern edges of the Atlantic and Pacific Ocean basins (Barriopedro et al., 2006; Croci-Maspoli et al., 2007; Dunn-Sigouin et al., 2013). In the Southern Hemisphere (SH), one main region of blocking exists, located southwest of South America (Renwick, 2005; Parsons et al., 2016; Brunner and Steiner, 2017). Overall, blocking occurs more frequently in the northern hemisphere than the southern. This difference in blocking frequency is assumed to related to the stronger stationary wave in the NH (Nakamura and Huang, 2018), often attributed to more prominent

midlatitude topography and land-sea contrasts, e.g., Held et al. (2002). However, to our knowledge, no study has confirmed this assumption.

Previous work suggests that the spatial distribution of blocking frequency (hereafter, the blocking climatology) is dependent on the behaviour of the stationary waves, jet streams, and storm tracks. Nakamura and Huang (2018) for example, propose that blocking is most ubiquitous in regions where the positive anomaly in the stationary wave maximizes, and mean westerly flow is weak. Work by others on the effects of transient eddy forcing on blocks (Shutts, 1983; Nakamura et al., 1997; Takaya and Nakamura, 2001; Wang and Kuang, 2019), shows the importance of the storm tracks. The work presented here aims to better characterize the manner in which the spatial distribution of the stationary waves, jet streams, and storm tracks are linked to the blocking climatology.

This article focuses on 4 main research questions:

1. Are blocks in an aquaplanet dynamically similar to blocks in orographically forced simulations and reanalysis?
2. Does the presence of orography affect the overall frequency of blocking?
3. How does orography affect the spatial distribution of blocking frequency?
4. Does orography affect the duration of blocking events?

To address question 1, we use compositing analysis to compare the life cycles of blocks for an aquaplanet, reanalysis and a model with orography. For questions 2 and 3, we compare the climatology of blocking, stationary waves, jet streams, and storm tracks for models with different orographic configurations. To answer question 4, we carry out an analysis that examines the sensitivity of block duration to mountains.

2 Methods

2.1 Reanalysis data

Although the focus of this paper is on idealized numerical modelling experiments, we also present results using reanalysis to motivate our work. The reanalysis used is the ECMWF ERA-Interim dataset (Dee et al., 2011). ERA-Interim (ERAI) has been shown to represent winter midlatitude storms as well as, and in some cases better than, other reanalyses (Hodges et al., 2011). Therefore, it likely does a reasonable job at capturing atmospheric blocking. ERA-Interim is produced using a model with roughly 0.67-degree resolution, but it is available to download at different resolutions. Herein, we used data with a 1.5 x 1.5 degree horizontal resolution. For this analysis we focus only on the cool season from 1979-2017, which is defined as Nov. – Mar., and May – Sept. for the Northern and Southern Hemispheres, respectively. Blocks are most abundant during these months (Tibaldi et al., 1994; Barriopedro et al., 2010).

2.2 Idealized model configuration

This work utilizes an idealized moist GCM described by Clark et al. (2018; 2019), which is modified from that introduced by Frierson et. al. (2006; 2007) and later altered by Frierson (2007) and O'Gorman and Schneider (2008). The

model is configured to use 30 unevenly spaced vertical sigma coordinate levels, and T42 spectral resolution, corresponding to 64 latitude by 128 longitude grid points when transformed to a latitude-longitude grid. Earth-like orbital parameters are used to simulate a full seasonal cycle in solar insolation. The model includes full radiative transfer and simplified physics parameterizations of convection (Frierson, 2007), boundary layer turbulence (Troen and Mahrt, 1986), and surface fluxes. There is no treatment of cloud radiative effects or condensed water in the atmosphere.

An aquaplanet configuration is run as the control integration. For the integrations with mountains, configurations of topographical forcing are simulated by modifying the model surface height and using a simplified treatment of land following Geen et al. (2017) and Vallis et al. (2018). Like Cook and Held (1992), and following Lutsko and Held (2016), perturbations to the surface height are introduced in the form of Gaussian mountains centered at 45˚ N with half-widths of 15 degrees in both the latitude and longitude dimensions. Several configurations are examined in this work:

a) Aquaplanet: idealized model with no orography
b) SingleMtn: 4 separate integrations with a single Gaussian mountain centered at 45° N, 90° E of variable peak height (1 km, 2 km, 3 km, 4 km respectively)
c) TwoMtn: 1 integration with two Asymmetrically placed 3 km high Gaussian mountains centered at 45° N, 90° E and 45° N, 150° W respectively. This placement is to loosely mimic the wide (Pacific) and short (Atlantic) zonal extents of the NH ocean basins.

The 3 km SingleMtn and TwoMtn configurations are shown in Figure 1. Ocean grid cells are represented using a slab ocean with a depth of 20 m. For simplicity we prescribe uniformly zero Q-flux, meaning that we assume that in the time mean, the net flux of energy from the ocean to the atmosphere is zero at all surface grid cells. In the configurations with mountains, land grid cells are defined as locations where the height is greater than 1/100th of the maximum surface height (3 km), corresponding to a height threshold of 30 m. As in Geen et al. (2017) and Vallis et al. (2018) land is simulated by reducing the slab ocean depth to 2 m (effectively reducing the heat capacity) and limiting evaporation using a bucket hydrology model. A uniform surface albedo of 0.26 is used to obtain a global annual mean surface temperature resembling that of the Earth. Each configuration is integrated for 40 years, but the first 10 years are discarded as spin-up time. Thus, the results presented here are for years 11-40 of each integration. 6-hourly data sets are used for the analyses in this paper, and the results are presented for Northern Hemisphere cool season, defined as the 5 months centered on the minimum in solar insolation. The model data is interpolated to the 1.5 x 1.5 degree horizontal ERA-Interim resolution prior to any analysis.

2.3 Block detection and tracking

Here we use a 500 hPa geopotential height (Z500) hybrid metric that utilizes the Z500 anomaly and meridional gradient. This metric was chosen for its robustness in terms of capturing high amplitude events involving wave-breaking (Dunn-Sigouin et al., 2013), and because it only requires the Z500 field – which simplifies tracking when analyzing large datasets. Barnes et al. (2012) finds that utilizing a Z500 metric produces similar blocking durations and climatologies to both potential vorticity and potential temperature based metrics. Blocks are detected and tracked using the algorithm described by

Dunn-Sigouin et. al. (2013), hereinafter as DS13, which is an adaptation of previous methods by Barriopedro et al. (2010) and Sausen et al. (1995). This algorithm searches for large, contiguous regions of persistent, high amplitude, positive anomalies in the Z500 field. Within these regions, Z500 must satisfy a meridional gradient reversal condition. What follows is an overview of the block identification algorithm, but specific details can be found in DS13:

1. Z500 Anomaly Calculation: For each grid-point poleward of 30 N, from the raw Z500 field subtract the running annual mean and mean seasonal cycle as computed in DS13.

2. Normalize each anomaly value by the sin of its latitude divided by sin of 45 degrees, i.e. $\frac{sin(\phi_{ij})}{sin(45°)}$, where ϕ_{ij} is the latitude of an arbitrary grid-point with longitude *i* and latitude *j*. This normalized anomaly will be referred to as Z500'.

3. For each month, in a 3-month window centered on a given month, calculate the standard deviation, S, of all Z500 ' values.

4. Amplitude threshold: Identify contiguous regions of positive Z500 'greater or equal to 1.5*S.

5. Size threshold: Regions must be at least 2.5 x 10^6 km^2 in area.

6. Gradient Reversal: The meridional gradient of the Z500 field within candidate regions must undergo a reversal in sign as described by DS13.

7. Quasi-stationary condition: For each timestep, regions must have a 50 % area overlap with its previous timestep (modified from DS13's 2 day overlap which was applied to daily mean data)

8. Blocks must meet the above criteria for at least 5 days (e.g. 20 6-hourly timesteps)

In case studies using ERAI and the idealized configurations described here, it was observed that two existing blocks sometimes merged with one another to form a single, larger block. We objectively identified this merging process based on extreme shifts in the location of the block centroid (defined as the gridpoint that is the centroid of the anomalous area associated with the block). If the centroid shifted by more than 1500 km from one 6-hourly snapshot to the next, we labelled the block as a merged event. These merged events represented 23-27 percent of the total initial blocks found in the idealized model integrations. We judge these events to be unique in terms of their relationship between block duration. Furthermore, the merger-blocks create uncertainty in terms of defining a block centre for the sake of our block-centered composite analysis. Therefore, we have excluded the merged events from our block-centered compositing and block duration analyses. The blocking climatological analysis on the other hand, retains all blocks since the primary focus is on the spatial distribution of block frequency, not the individual blocks themselves.

2.4 Analysis metrics

The metrics used to characterize climatological features and blocking in the idealized model data and reanalysis are outlined below.

2.4.1 Stationary Wave and Eulerian Storm Track

The cool season stationary wave at each point is defined as the anomaly with respect to the zonal mean of the cool season climatology for the 250-hPa geopotential height field: $\bar{Z}^* = \bar{Z} - \left[\bar{Z}\right]$, where brackets indicate the zonal mean and overbar indicates the time mean over cool season days for all years. This is computed separately for each gridpoint.

The Eulerian storm track is presented as the standard deviation of a 24-hour difference of the daily mean Z500 field during cool season (Wallace et al., 1988; Guo et al., 2009; Booth et al., 2017). Consider $Z_{500}(t)$ to be the daily mean Z500 value for an arbitrary gridpoint. To obtain the storm track:

1. The 24-hour difference, Z_{500}^{τ}, at each gridpoint is taken as:

$$Z_{500}^{\tau} = Z_{500}(t+1) - Z_{500}(t)$$

2. Then, the standard deviation of Z_{500}^{τ} for all cool season timesteps at each gridpoint is taken to obtain the cool season Eulerian storm track value at that point.

This is computed separately for each gridpoint.

2.4.2 Blocking and Zonal Wind Climatologies

The spatial distributions of blocking frequency, referred to hereinafter as the blocking climatologies, are calculated by averaging the block identification flag (1 or 0 respectively) per gridpoint over all cool season days. Thus, the blocking climatologies show the percent of cool season timesteps a block (as defined here) is present. This is computed separately at each gridpoint.

The 250 hPa zonal wind climatology, hereinafter referred to as $\overline{U250}$, is presented as the time mean of the 250-hPa zonal wind over the cool season months at each gridpoint.

2.4.3 Wave activity flux vectors

To better characterize the dynamical evolution of blocks within each model, wave activity flux vectors (hereinafter, $\vec{\boldsymbol{W}}$) are calculated as described by Takaya and Nakamura (2001), hereinafter TN01. The wave activity flux relates eddy feedback onto the mean state and is essentially the pseudo-momentum associated with Rossby waves. Convergence of $\vec{\boldsymbol{W}}$ is associated with blocking and an overall slowing or reversal of westerly flow. The formulation of $\vec{\boldsymbol{W}}$ in TN01, includes a stationary term that dominates for quasi-stationary, low frequency eddies (i.e. 8- to 30-day timescales), and a non-stationary, group-velocity dependent term that is more relevant for higher frequency eddies. Here we calculate only the stationary, horizontal component of $\vec{\boldsymbol{W}}$, and focus on contributions solely from the low frequency eddies.

Block centered composites (as described in Sect. 2.5.1. of this paper) are computed using $\vec{W}$ for each block during various stages of the block's lifecycle. The horizontal components of $\vec{W}$ are calculated as in TN01. For this, eddy fields are computed with an 8- to 30-day bandpass filter. This is what is described as low frequency eddies in TN01 and Nakamura et al. (1997). $\vec{W}$ are given by:

$$\vec{W} = \frac{p\cos\phi}{2|\vec{U}|}\begin{pmatrix} U\left(v'^2 - \frac{\Phi'}{f}\frac{\partial v'}{\partial x}\right) + V\left(-u'v' + \frac{\Phi'}{f}\frac{\partial u'}{\partial x}\right) \\ \square \\ U\left(-u'v' + \frac{\Phi'}{f}\frac{\partial v'}{\partial y}\right) + V(u'^2 + \frac{\Phi'}{f}\frac{\partial u'}{\partial y}) \end{pmatrix}$$

This calculation is performed on variables on the 250-hPa pressure surface. For each point p is the pressure and ϕ is latitude. $\vec{U}$ is the 30-day low-pass filtered horizontal wind vector with zonal and meridional components U and V, respectively. The anomalous zonal wind, meridional wind, and geopotential are given by u', v',and Φ', respectively. Derivatives are computed using finite-differencing, where zonal derivatives are weighted by latitude. $\vec{W}$ are given in m^2s^{-2}.

2.5 Analysis methods

2.5.1 Block-centered compositing

The Z500', $\vec{W}$, and $\nabla \cdot \vec{W}$ fields are composited around the centroid of each block for the first, strongest, and final days of each block lifecycle. To account for the convergence of meridians, relevant fields are projected onto equal-area grids before compositing. The initial time step of a block is the first timestep that the block satisfies the amplitude, size, and reversal conditions. The strongest time step of a block is defined as the time step with the greatest Z500 '(at a single lat/lon location) within a block. The final timestep is the last timestep a block satisfies the amplitude, size, and reversal conditions.

The composites presented in this paper, only include midlatitude-blocks whose centroid are always south of 65˚ N. This is because we find that the high-latitude blocks exhibit distinct physical behaviour. From reanalysis data, high-latitude blocks in the Southern Hemisphere have different dynamical evolution and different impacts on the surrounding flow, as compared to midlatitude blocks (Berrisford et al., 2007). The 65˚ N cut-off was chosen after estimates showed this to be near the minimum in the meridional potential vorticity gradient, and thus the northern limit of the midlatitude waveguide (e.g. Wirth et al. 2018). Compositing results were robust to changes in cut-off latitude of +/- 7.5˚.

2.5.2 Separating blocks by region

To compare the dynamical evolution of blocks originating near the eastern edge of the ocean basins (denoted as "East", near the windward side of mountains and the high-pressure maxima of stationary waves) against blocks originating elsewhere (denoted as "Other"), blocks are sorted by their centroid location during their first timestep. These regions are

outlined in Table 1 and shown in Figure 1. The East region spans 30˚-65˚ N for 90 degrees of longitude upstream and inclusive of the mountain centre. For the TwoMtn configuration, "East" and "Other" refer to two regions within the zonally larger ocean basin (which we refer to as the "Wide Basin"), whereas blocks originating within the zonally smaller ocean basin are denoted as from the "Short Basin".

2.5.3 Block duration probability density distributions

Block duration is defined as the time interval from the initial identification timestep to the end of that block's existence – based on the block identification algorithm (described in Sect. 2.3). Each block is thus assigned one duration value. The steps taken to obtain block duration probability density distributions are as follows:

1. Sort blocks into subsets by model configuration and/or basin.
2. Allowing replacement, randomly select a set of block durations within a given subset. The size of the random set is given by the number of blocks in the subset being analysed.
3. Place the durations yielded by step 2 into n equal sized bins (n=8 for figures in this paper) ranging from the minimum to maximum duration of cool season blocks between all model configurations.
4. Steps 2 and 3 are then repeated m times (m=1000 for figures in this paper) to produce an ensemble of m probability density distributions for each subset.
5. For a given subset, the mean probability density distribution is computed by taking the mean of that subset's distributions. This is then smoothed using a running mean.
6. For a given subset, the standard deviation of probability density distribution is computed by taking the standard deviation of that subset's distributions

The results of this paper are nearly constant with respect to changes in the values of n (+/- 2) and m (+/- 200). For all configurations, distributions and mean values presented for duration exclude any high-latitude blocking (blocks whose centroid are ever poleward of 65° N). 65° N was found to be the most appropriate cut-off in each configuration for the same reasons as described for the aquaplanet compositing.

2.5.4 Statistical significance

For a given gridpoint and cool season, a block frequency value is computed by averaging all the block identification flag values (1 or 0) for each timestep of that cool season. This is done at every gridpoint for every cool season to yield a 3D matrix of dimensions latitude by longitude by number of years. 2-sample t-tests are then performed for corresponding gridpoints between a given topographic configuration and a 250-year aquaplanet integration. A 250-year aquaplanet integration is used because the blocking climatology is more zonally symmetric when compared to climatology calculations that use less years. This is done to identify regions of enhanced and suppressed blocking frequency in the topographic integrations. Significance testing in hemispherically averaged block frequency statistics are done by calculating area averaged blocking frequency for each cool season. For each configuration, this yields a one-dimensional array of values for each cool season. A

2-sample t-test is then used to examine significant differences in hemispherically averaged block frequency between idealized model configurations. Significance testing for mean block duration also utilizes a 2-sample t-test to compare differences between the various configurations and regions. A 95% confidence interval is imposed as the significance threshold for all significance testing.

3 Results

3.1 Blocking in the aquaplanet, dynamical aspects

On average, 12.9 blocks per cool season are identified for each hemisphere of the aquaplanet. The presence of blocking in this model configuration is consistent with previous studies that also find blocking in GCM's with zonally symmetric forcing (Hu et al., 2008; Hassanzadeh et al., 2014, Nabizadeh et al., 2019). Figure 2 shows a snapshot of the first day of an arbitrary block in the aquaplanet. Upstream and coincident with the block, a Rossby wave pattern can be observed in both the Z500 and Z500 ′fields (Fig. 2 - the Z500 contours show a wave-like feature, and the Z500 ′field shows an alternating pattern of low and high anomalies in the zonal direction). The presence of these features during the formation of a block agrees with previous work for both simplified (Berggren et al., 1949; Rex, 1950; Colucci, 1985; Nakamura et al., 1997; Hu et al., 2008), and comprehensive models (TN01; Yamazaki and Itoh, 2013; Nakamura and Huang, 2018; Dong et al., 2019).

In Figure 2 near 75-85° W, a characteristic overturning of the Z500 contours indicative of anticyclonic Rossby wave breaking (Masato et al., 2012; Davini et al., 2012) is also observed. Concentrated, large magnitude $\vec{\boldsymbol{W}}$ are found just upstream of, and propagating into the block, and a relative absence of large magnitude $\vec{\boldsymbol{W}}$ occur downstream of the block. On the upstream, equatorward flank of the block, converging $\vec{\boldsymbol{W}}$ consistent with a slowing of the zonal mean flow is observed. The behavior of $\vec{\boldsymbol{W}}$ during the genesis of this block case study agrees with Nakamura et al. (1997) and TN01 and is consistent with Nakamura and Huang's (2018) description of blocking as a traffic jam of wave activity fluxes.

Block-centered compositing analysis is used to confirm that, on average, the blocks identified in the aquaplanet model evolve in a dynamically similar manner to models with zonally asymmetric forcing. Figure 3 shows block centered composites of Z500', $\vec{\boldsymbol{W}}$, and $\nabla \cdot \vec{\boldsymbol{W}}$ for blocks in the SH midlatitudes (i.e., occurring between 30˚ and 65˚ of latitude) of ERA-Interim (ERAI SH, left column, Figs. 3a-c), the aquaplanet midlatitudes (middle column, Figs. 3d-f), and the East region (see table 1 and figure 1) of the 3 km single mountain configuration (3 km SingleMtn East, right column, Figs. 3g-i). ERAI SH was chosen to avoid the regional variation found in NH blocking (Nakamura et al., 1997; Davini et al. 2012), however, we remind the reader that surface forcing in the SH is asymmetric (e.g. Berrisford et al. 2007). 3 km SingleMtn East blocks were chosen to subset blocks into those that form near the high-pressure anomaly of stationary waves. Only the 3 km SingleMtn East results are shown because block-centered composites for the different topographic configurations (i.e. 1 km, 2 km, 3 km, and TwoMtn), and "Other" regions yielded similar results (not shown).

The onset of blocking (Fig. 3 top row) in the aquaplanet composite (Fig. 3d) is qualitatively similar to that found in the case study (Fig. 2), ERAI SH (Fig. 3a), and SingleMtn 3k East (Fig. 3g). Minor differences are observed however, such as stronger upstream Z500' gradients in ERAI SH and SingleMtn 3k East, and weaker $\vec{W}$ convergence in SingleMtn 3k East. For composites over blocks at maximum strength (Fig. 3 middle row), a similar pattern of $\nabla \cdot \vec{W}$ is observed between the 3 models (Figs. 3b, 3e, and 3h). Convergence of $\vec{W}$ on the downstream, equatorward flank of the composite blocks are enhanced compared to onset, and the envelope of greatest $\vec{W}$ is now within the high-pressure center. Upstream, downstream, and equatorward low-pressure centers are also evident when the composite blocks are at peak strength, though the pattern is not as clean in idealized model composites (Figs. 3e and 3h) compared to ERAI SH (Fig. 3b). Also, the equatorward cyclone in ERAI SH (Fig 3b) is further upstream than in the idealized cases.

On the final day (bottom row, Figs 3c, 3f, and 3i), each respective composite block's Z500 anomaly weakens, and low-pressure is concentrated downstream from the block. Weak values of $\vec{W}$ exit the block downstream of the high-pressure maximum during this time (Fig. 3c, 3f, 3i). This is all consistent with downstream development (Danielson et al., 2005). A net divergence of $\vec{W}$ from the blocked region is indicative of a return to westerly zonal flow as the block dies out.

The block-centered composites for the aquaplanet are qualitatively similar to composites for ERAI SH, and the idealized model configurations with mountains in terms of the evolution of Z500', $\vec{W}$, $\nabla \cdot \vec{W}$. The likeness of the aquaplanet to ERAI SH is interesting due to the idealized conditions in the model, as well as the lack of topography. These results show the potential utility of an aquaplanet model for understanding the fundamental physics of blocking. The similarities between blocks in the aquaplanet and the topographic configurations show that blocks behave in a similar manner with or without mountains as a source of zonally asymmetric forcing. Having shown that individual blocking events behave as expected in the idealized model, we now shift our focus to the climatological flow features and blocking climatology.

3.2 Climatological Analysis

The majority of theories on blocking formation and maintenance (summarized in the review by Woollings et al. 2018) imply that stationary waves, storm tracks, and upper level mean flow all might play important roles setting the spatial distribution of blocking frequency. These quantities are now examined for the aquaplanet, reanalysis, and model integrations with mountains. In our discussion of the climatological features in reanalysis and the SingleMtn configurations, we have chosen the following approach: we first discuss the stationary wave because it is the most fundamental metric that changes when adding mountains; then, we discuss blocking and its relationship to the jet stream. We close the analysis with a discussion of the storm tracks. This choice of the order is motivated by recent theory from Nakamura and Huang (2018) that put greater emphasis on the influence of the jet stream and stationary waves on blocking.

3.2.1 The aquaplanet

For the aquaplanet, the stationary wave, storm track, and $\overline{U250}$ are zonally symmetric (Figs. 4a and 4b). However, the blocking climatology is not zonally symmetric after 30 years (Fig. 4b). We find that it takes 250 years for the aquaplanet blocking climatology to approach zonal symmetry (Figs. 4c and 4d). However, for the models with orography, the time to reach convergence is likely not as large. We deduced this from the following analysis: we generate 20-year climatologies using randomly sampled years from our 30-year integrations and compare them. For the for the configurations with orography, the blocking climatology is spatially consistent, whereas, for the aquaplanet, each climatology has a unique spatial distribution (not shown). Therefore, we believe that 30-years of model runs provides a usable level of convergence of the spatial climatology of blocking in the integrations with mountains.

3.2.2 Reanalysis

The different orographic configurations of the northern and southern hemispheres produce distinct spatial distributions of general circulation features and atmospheric blocking (Fig. 5). Stationary wave patterns can emerge due to land-sea heating contrasts, drag, and flow deflection by topography (e.g. Held et al., 2002). The two strongest regions of anomalous high-pressure in the NH are located on the windward side of the Rocky Mountains, and near the western edge of Europe (Fig. 5a). In the SH, the high-pressure maximum is southwest of South America, and a secondary maximum can be found southeast of Australia (Fig 5b). These results are consistent with previous work (Valdes and Hoskins, 1991; Quintanar and Mechoso, 1995; Held et al., 2002; White et al., 2017).

Near the high-pressure stationary wave maxima (Figs. 5a-b), regions of suppressed $\overline{U250}$ are apparent (Figs. 5c-d). These regions have been shown to be regions of local maxima for Rossby wave breaking (Abatzoglou and Magnusdottir, 2006; Bowley et al. 2018). These regions are also where blocks are found to occur most often (Figs. 5c-d), in agreement with previous work (Wallace et al., 1988; Barriopedro et al., 2006; Dunn-Sigouin, 2013; Brunner and Steiner, 2017). According to Nakamura and Huang (2018), strong positive stationary wave anomalies, and weak mean westerlies are conducive to blocking. These conditions act to slow down the "speed limit" on $\vec{\boldsymbol{W}}$, leading to "traffic jams" manifested as blocking episodes. Conversely, regions of strong westerlies, and negative stationary wave anomalies have an opposite effect, hence the suppression of blocking in regions of maximal $\overline{U250}$ (Figs. 5c-d) near climatological lows (Figs. 5a-b).

Focusing next on storm tracks, we see that the entrance of the storm tracks occurs on the northeast edge of the $\overline{U250}$ maxima (Fig. 5a, 5c). The details for this relationship are discussed in Chang et al. (2002) and explored in detail for the N. Atlantic in Brayshaw et al. (2009). In the SH, there are also two local maxima in the storm tracks, and they occur to the southeast of the respective $\overline{U250}$ maxima. At the storm track exit region, transient eddies play an important role in the onset (Colucci 1985) and maintenance of blocks (Shutts, 1983; Nakamura et al. 1997; Yamazaki and Itoh 2013; Pfahl et al. 2015; Wang and Kuang, 2019). This region is also where the stationary wave and blocking maxima occur (Fig. 5). There is one

exception in the SH however: the SH storm track exit at the eastern terminus of the Indian Ocean (i.e., 90˚ E) does not coincide with a maxima in blocking or the stationary wave – but it is a region of locally weak $\overline{U250}$.

For the NH (SH) in this dataset, 485 (336) blocking events are found yielding a hemispherically-averaged blocking frequency of 2.7 % (1.6 %). The greater amount of blocking in the NH is typically assumed to be a result of the relative abundance of topographic features. Therefore, we will use configurations of the model to explore the effects of mountains on the spatial distribution and hemispherically averaged statistics of blocking frequency.

3.2.3 Orographic Configurations: Single Mountain of varying height

Here, a single mountain is added to the aquaplanet to study the response of the idealized model blocking climatology to the presence of orography. Figure 6 shows the stationary waves, storm tracks, blocking climatologies, and $\overline{U250}$ in the SingleMtn integrations. In each integration, a stationary wave is induced (Figs. 6a-6d) with a high-pressure anomaly generated near the coastline on the windward side of the mountain, and a low-pressure anomaly on the leeward side (Fig. 6a-d). This results in a meridionally tilted stationary wave pattern that extends into the subtropics leeward of the mountain. This pattern has been explained in previous idealized modeling work (Grose and Hoskins, 1979; Cook and Held, 1992; Lutsko 2016). The intensity and zonal extent of the stationary wave extrema increases with mountain height (Figs. 6a-d).

In the SingleMtn integrations, as the height of the mountain is increased, the local maximum in the $\overline{U250}$ increases as well (right column, Fig 6). This relationship between the strength of the local jet maxima and mountain height follows from the thermal wind relationship and the increased temperature gradient in the lower troposphere downstream of the mountain. This mechanism is also apparent in Brayshaw et al. (2009). The stronger temperature gradient is due to enhanced cold advection in the runs with taller mountains. This pattern of the $\overline{U250}$ maximum occurring just downstream of mountains is the same as what occurs for the NH in observations (Fig. 5a). Across models, localized strengthening near the maximum $\overline{U250}$ is accompanied by a weakening of $\overline{U250}$ further downstream. In regions poleward of the midlatitude minimum in $\overline{U250}$, blocking is most abundant (Figs. 6e-h). This region also coincides with the high-pressure maximum of the stationary wave (Figs. 6a-d). The weakened flow and positive stationary wave anomaly here are consistent with a region of lowered $\vec{\boldsymbol{W}}$ "speed limit" (Nakamura and Huang, 2018), and thus enhanced block frequency. Figures 6e-h shows that these regions have significantly more blocking compared to the extended aquaplanet run. On the other side of the mountain, block frequency is significantly suppressed near the low-pressure stationary wave anomaly, poleward of the $\overline{U250}$ maximum.

The presence of mountains also leads to localized storm track maximum in each of the SingleMtn configurations (Figs. 6a-d). The storm track maximum straddles the stationary wave minimum immediately downstream of the region where the $\overline{U250}$ maximum also occurs (Fig. 6e-h). The storm track exit region in the idealized model does not coincide with the high-pressure stationary anomaly, as it does in the NH of Earth. This allows one to work toward decoupling the response of blocking to each feature. The main blocking maximum occurs near the stationary wave maximum, which is 60˚ longitude east

of the storm track exits. Near the storm track exit region, where the stationary waves are near neutral (i.e. near 90 W), there are suggestions of secondary blocking maxima (Fig. 6e-h). This region is perhaps related to the breaking of Rossby waves at the end of the storm track and a local block genesis region associated with strong extratropical cyclones. This would be consistent with theories linking blocking to Rossby wave-breaking (Pelly and Hoskins, 2003; Berrisford et al., 2007; Masato et al. 2012).

The zonal extent of the blocking climatology maximum increases when mountain height is increased (Figs. 6e-h). This agrees with the response of the stationary wave (Figs. 6a-d). The overall hemispherically averaged statistics of blocking frequency yields an increase in blocking when mountain height is increased (See Table 2). These increases for the 2k-4k configurations are modest however and should be taken with some degree of caution. Still, it is clear that as mountain height increases, there is a greater area of significantly more blocking compared to the aquaplanet (Figs. 6e-h). Next, we investigate the response of adding an additional mountain.

3.2.4 Topographic Configurations: 2 Mountains

For this analysis, two 3 km-high Gaussian mountains centered at 45° N with 120° of longitude between them are added to the aquaplanet. The placement of the mountains is meant to create a wide and short ocean basin, as observed in the NH of earth. 3 km height is meant to be semi-realistic; the values are lower than the maxima for the Rockies and the Himalayas – however the mountains are substantial enough to have generate obvious changes in the circulation (as evidenced in the Single Mountain experiments).

The addition of a second mountain induces a second trough and ridge in the stationary wave, and a second maxima for the blocking climatology, storm track, and $\overline{U250}$ (Fig. 7). The intensity and zonal extent of these features, however, varies with respect to each mountain and is a result of interference between the forcing (Manabe and Terpstra, 1974; Held et al., 2002; White et al., 2017).

The TwoMtn configuration has a greater hemispherically averaged blocking frequency than the other configurations (Table 2). This is despite the TwoMtn configuration having a lower total number of blocks than the 3 and 4 km SingleMtn configurations, respectively – meaning the blocks have a longer average duration in the 2-mountain configuration (Table 3). Each mountain also creates regions of enhanced and suppressed blocking frequency (Fig. 7b). However, just like the general circulation features, there are differences in the blocking climatology for the two ocean basins.

Next, we examine the blocking climatology within each of the two ocean basins in the TwoMtn simulation (Wide Basin and Short Basin, respectively, see Fig. 1 and Table 1). In the Wide Basin, there is close to a basinwide enhancement of blocking frequency when compared to the single mountain cases (Figs. 6e-h, and 7b). Consistent with this enhancement, the overall midlatitude $\overline{U250}$ climatology is much weaker in the wide basin compared to the other ocean basin and SingleMtn integrations. In the Short Basin, a separate blocking maximum exists near the high-pressure stationary wave anomaly. This

maximum, albeit much weaker than its wide basin counterpart, is still significantly more than what occurs in the same region for the aquaplanet.

The proximity of the storm track maximum in the short basin makes there more likely to be times in which storm development occurs just upstream of the mountain; this coupled with a strong background westerly flow would inhibit blocking and perhaps explains the discrepancies between the wide basin and short basin maxima. The shorter ocean basin containing much less blocking is not consistent with what is observed in the NH of Earth, where the Atlantic has a slightly stronger blocking maximum. It seems more elaborate landmasses than this simplified case are needed to better simulate what is observed between the Atlantic and Pacific blocking climatologies in the NH.

3.3 Block Duration Statistics

One of the characteristics that allows blocks to influence midlatitude weather is their persistence. As such, we examine the influence of mountains on block persistence using our duration metric. First, we find that adding mountains leads to at least a modest increase in the average midlatitude block duration (Table 3). All topographic configurations aside from 1 km SingleMtn, also have 7-39 more blocks than the aquaplanet (Table 3). This helps to explain some of the climatological differences in block frequency between the idealized model configurations (Table 2), particularly for the 1 km SingleMtn case. Despite a 0.25 day greater mean block duration (Table 3), 1 km was found to have less hemispherically averaged blocking than the aquaplanet (Table 2) due to 21 less events. The blocks in the topographic integrations were then put into subsets based off those originating near the high-pressure stationary wave anomaly and those that were not.

Regions used to subset blocks are denoted as “East”, those originating at the eastern end of the ocean basin near the high-pressure stationary anomaly, and “Other”, those originating elsewhere in the midlatitudes (Fig. 1a and Table 1). Figure 8 shows the probability density functions for the aquaplanet and SingleMtn East blocks. With the exception of the 4 km run, the “East” regions of the single mountain integrations have relatively less shorter duration blocks (i.e. 5-11 days), and relatively more longer duration blocks (11 days or more) compared to the aquaplanet (Fig. 8). Blocks from the “East” regions last longer on average than aquaplanet blocks (Table 3), but the 3 km and 4 km enhancement of block duration are not significant to the 95th percentile. Mean block duration is greater for the “East” region compared to the “Other” in the single mountain configurations (Table 3), with significant differences found in the 1 km and 2 km integrations. This leads to a cautious suggestion that blocks that originate near mountains last longer on average than those that do not, though the modest differences found in the 3 km and 4 km integrations must be considered.

The response of the TwoMtn configuration is much less straightforward. This integration is divided into 3 regions, Wide Basin East, Wide Basin Other, and Short Basin (Fig. 1b and Table 1); Note the Short Basin does not have distinct “East” and “Other” regions because of its shortened zonal extent. Average block duration in the “Other” region in the Wide Basin is slightly longer than the “East”, but both regions are significantly greater than the Short Basin. This coupled with more Wide Basin East events (Table 3) is consistent with the weaker maximum in the blocking climatology for the Short Basin (Figure

7b). Perhaps this is related to the inhibition of blocking by the nearby storm track and $\overline{U250}$ maximum in the Short Basin, but we do not seek to attribute a causal relationship here.

Our results suggest that blocks starting near mountains last longer on average than those that do not (Table 3). In reality we see a similar situation where the NH has more orographic forcing compared to the SH, and also a longer average block duration (8.0 days for the NH and 6.9 days for the SH). In the idealized model, the compositing analysis for the aquaplanet shows similar forcing patterns by low frequency eddies ($\overline{\nabla \cdot \vec{\boldsymbol{W}}}$) when compared to the SingleMtn East blocks (Figs. 3d-i), despite having a shorter average block duration. Perhaps these duration differences can be accounted for by considering block maintenance by high frequency transients (Shutts, 1983; Nakamura et al., 1997; TN01; Yamazaki and Itoh, 2013; Wang and Kuang, 2019). High frequency eddy forcing has yet to be investigated in these experiments, but this will be a topic of future work.

4. Discussion

To add some perspective on the role of mountains as compared to land masses with no orographic features, we analyze the response of an idealized model configuration with a single flat land mass, herein referred to as 0 km (Fig. 9). The results of 0 km are briefly mentioned here to primarily serve as a benchmark for this setup. This configuration is like the others that include mountains in that it imposes zonally asymmetric forcing in land-sea contrast and orographic drag (Pithan et al., 2016); The difference, however, is that that the flat land does not act a direct barrier that deflects the flow as the mountains do, generating a unique stationary wave response (e.g. Held et al. 2002) (Figs 6a-d, 7a, and 9).

The response of $\overline{U250}$ and the storm track (Fig. 9) in 0 km agree with results by Brayshaw et al. (2009). Compared to the single mountain runs, the stationary wave pattern is shifted upstream in 0 km (Figs. 6 and 9). The blocking climatology maximizes (minimizes) poleward of regions where the midlatitude $\overline{U250}$ minimizes (maximizes) (Fig. 9b). In the single mountain integrations, the maximum in the blocking climatology is nearly co-located with the maximum in the stationary wave; For the 0 km integration, it is not. The high-pressure stationary anomaly seemingly plays less of a role in the flat case. The 0 km integration has a 3.42 % hemispherically averaged block frequency, which is greater than the aquaplanet and 1 km configurations but less than the others with taller mountains (Table 2).

5. Summary and conclusions

This work utilizes an idealized moist GCM to better understand atmospheric blocking. We start with an analysis of blocking in an aquaplanet, then systematically add mountains to investigate the influence of orography on blocking frequency and duration.

Using the aquaplanet we confirm that blocks can be generated purely through eddy-eddy interactions, without any zonally asymmetric forcing from the surface. This result substantiates the results of Hu et al. (2008), Hassanzadeh et al. (2014),

and Nabizadeh et al. (2019). To expand on the results of those previous studies, we examined the dynamical life cycle of the blocks in the aquaplanet. Block centered composites of Z500 ’and $\vec{W}$ show that block lifecycles in the aquaplanet include:

(1) Large-scale Rossby wave features with $\vec{W}$ entering the block and converging on the upstream-equatorward flank during onset

(2) Stronger $\vec{W}$ convergence and greater concentrations of $\vec{W}$ inside the block during peak strength

(3) A net divergence of $\vec{W}$ emitted downstream of the block into low-pressure regions during decay

Similar behaviour is shown for reanalysis and the idealized model configurations that include orography, affirming the usefulness of a simple idealized aquaplanet model in better understanding blocks observed in reality.

In experiments with orographic forcing, we modified the aquaplanet model in the following ways: (1) adding a single mountain of different heights in separate integrations; and, (2) in another integration, adding two 3-km high mountains placed in a manner that creates one wide and one short ocean basin. The addition of mountains to the idealized model led to several changes in blocking when compared to the aquaplanet integration:

- There are localized maxima in blocking, upstream of mountains; near the high-pressure maximum of the stationary waves; poleward and near climatological minima in $\overline{U250}$.
- There are localized minima in blocking, downstream of mountains; near the low-pressure anomaly of the stationary wave; poleward and near climatological maxima in $\overline{U250}$.
- There is a significant increase in hemispherically averaged blocking frequency in integrations with mountains of height 2 km and greater.
- There is an increase in block duration for blocks originating near mountains, though the statistics are not robust.

Based on ERA-Interim reanalysis, these results mirror what is observed for the NH and SH, where the NH contains more topography and blocking. In the idealized model, the enhancement of block frequency near the stationary wave maximum and $\overline{U250}$ minimum is consistent with these regions being conducive to the convergence (or “traffic jamming”) of wave activity fluxes. These regions are found to be far from the storm track exit however, which is dissimilar to the NH in reanalysis. At the storm track exit region in the North Atlantic, previous work has shown that extratropical cyclones can seed blocks (Colucci 1985) or maintain them, Pfahl et al. (2015). However, the storm track exit coincides, or sits spatially close to the stationary wave maxima. In our single mountain experiments, the storm track exit is far from the stationary wave maxima, and the result is that the blocks preferentially occur at the stationary wave maxima region. This suggests that the role of the cyclones in nature may be secondary to the role of the large-scale flow. That being said, secondary blocking maxima are found near the storm track exit in the idealized model, suggesting that this location also plays a key role in anchoring where blocks most frequently occur.

Overall, this work elucidates fundamental information on the formation, dynamical evolution, spatial distribution,

and duration of atmospheric blocking – both in an aquaplanet and configurations with zonally asymmetric forcing. One limitation in the two-mountain experiment, is that each mountain simultaneously affects the stationary wave, jet, and storm track, making it difficult to tell the order of influence each has on the blocking climatology. Understanding the interplay and individual effects of these flow features is key to predicting the behavior of blocks in future climates. This is a topic of future work.

Acknowledgements:

This study is supported and monitored by The National Oceanic and Atmospheric Administration – Cooperative Science Center for Earth System Sciences and Remote Sensing Technologies under the Cooperative Agreement Grant #: NA16SEC4810008. The authors would like to thank The City College of New York, NOAA Center for Earth System Sciences and Remote Sensing Technologies, and NOAA Office of Education, Educational Partnership Program for fellowship support for Veeshan Narinesingh, and the American Society for Engineering Education for their support of Spencer K. Clark through a National Defense Science and Engineering Graduate Fellowship. The statements contained within the manuscript are not the opinions of the funding agency or the U.S. government, but reflect the authors 'opinions.

References

Abatzoglou, J. T., and Magnusdottir, G.: Planetary Wave Breaking and Nonlinear Reflection, J. Climate, 19, 6139-6152, doi:10.1175/JCLI3968.1, 2006.

Barnes, E., Slingo, J., and Woollings, T.: A methodology for the comparison of blocking climatologies across indices, models and climate scenarios. Clim. Dynam., 38, 2467-2481, doi:10.1007/s00382-011-1243-6, 2012.

Barriopedro, D., GarcÍa-Herrera, R., Lupo, A. R., and Hernández, E.: A Climatology of Northern Hemisphere Blocking. J. Climate, 19, 1042-1063, doi:10.1175/JCLI3678.1, 2006.

Barriopedro, D., García-Herrera, R., and Trigo, R.: Application of blocking diagnosis methods to General Circulation Models. Part I: a novel detection scheme. Clim. Dynam., 35, 1373-1391, doi:10.1007/s00382-010-0767-5, 2010.

Berggren, R., Bolin, B., and Rossby, C.-G.: An Aerological Study of Zonal Motion, its Perturbations and Break-down. Tellus, 1, 14-37, doi:10.3402/tellusa.v1i2.8501, 1949.

Berrisford, P., Hoskins, B. J., and Tyrlis, E.: Blocking and Rossby Wave Breaking on the Dynamical Tropopause in the Southern Hemisphere. J. Atmos. Sci., 64, 2881-2898, doi:10.1175/JAS3984.1, 2007.

Booth, J. F., Dunn-Sigouin, E., and Pfahl, S.: The Relationship Between Extratropical Cyclone Steering and Blocking Along the North American East Coast. Geophys Res. Lett., 44, 11-11,984, doi:10.1002/2017GL075941, 2017.

Booth J. F., Kwon, Y.-K., Ko, S., Small, J., Madsek, R.: Spatial Patterns and Intensity of the Surface Storm Tracks in CMIP5 Models. Journal of Climate, 30, 4965–4981. 2017.

Bowley, K. A., Gyakum J. R., and Atallah E. H.: A New Perspective toward Cataloging Northern Hemisphere Rossby Wave Breaking on the Dynamic Tropopause. Mon. Weather Rev., 147, 409-431, doi:10.1175/MWR-D-18-0131.1, 2019

Brayshaw, D. J., Hoskins, B., and Blackburn, M.: The Basic Ingredients of the North Atlantic Storm Track. Part I: Land–Sea Contrast and Orography. J. Atmos. Sci., 66, 2539-2558, doi:10.1175/2009JAS3078.1, 2009.

Brunner, L., Schaller, N., Anstey, J., Sillmann, J., and Steiner, A.: Dependence of Present and Future European Temperature Extremes on the Location of Atmospheric Blocking. Geophys. Res. Lett., 45, 6311-6320, doi:10.1029/2018GL077837, 2018.

Brunner, L., A. Steiner, 2017: A global perspective on atmospheric blocking using GPS radio occultation – one decade of observations. Atmospheric Measurement Techniques, 10, 4727-4745, doi:10.5194/amt-10-4727-2017.

Cassou, C., Terray, L. and Phillips, A. S.: Tropical Atlantic Influence on European Heat Waves. J. Climate, 18, 2805-2811, doi:10.1175/JCLI3506.1, 2005.

Charney, J. G., DeVore, J. G.: Multiple Flow Equilibria in the Atmosphere and Blocking. J. Atmos. Sci., 36, 1205-1216, doi:10.1175/1520-0469(1979)036<1205:MFEITA>2.0.CO;2, 1979.

Clark, S. K., Ming, Y., Held, I. M., and Phillips, P. J.: The Role of the Water Vapor Feedback in the ITCZ Response to Hemispherically Asymmetric Forcings. J. Climate, 31, 3659-3678, doi:10.1175/JCLI-D-17-0723.1, 2018.

559 Clark, S. K., Ming, Y., and Adames, Á. F.: Monsoon low pressure system like variability in an idealized moist model. J.
560 Climate. doi:10.1175/JCLI-D-19-0289.1, 2019.
561 Colucci, S. J.: Explosive Cyclogenesis and Large-Scale Circulation Changes: Implications for Atmospheric Blocking. J.
562 Atmos. Sci., 42, 2701-2717, doi:10.1175/1520-0469(1985)042<2701:ECALSC>2.0.CO;2, 1985.
563 Cook, K., Held, I. M.: The Stationary Response to Large-Scale Orography in a General Circulation Model and a Linear Model.
564 J. Atmos. Sci., 49, 525-539, doi:10.1175/1520-0469(1992)049<0525:TSRTLS>2.0.CO;2, 1992.
565 D'Andrea, F., Tibaldi, S., Blackburn, M., Boer, G., Déqué, M., Dix, M. R., Dugas, B., Ferranti, L., Iwasaki, T., Kitoh, A.,
566 Pope, V., Randall, D., Roeckner, E., Strauss, D., Stern, H., Van den Dool, W., and Williamson, D.: Northern
567 Hemisphere atmospheric blocking as simulated by 15 atmospheric general circulation models in the period 1979–
568 1988. Clim. Dynam., 14, 385-407, doi:10.1007/s003820050230, 1998.
569 Danielson, R. E., Gyakum, J. R., Straub D. N.: A Case Study of Downstream Baroclinic Development over the North Pacific
570 Ocean. Part II: Diagnoses of Eddy Energy and Wave Activity. Mon, Weather Rev., 134, 1549-1567,
571 doi:10.1175/MWR3173.1, 2006
572 Davini, P., Cagnazzo, C., Gualdi, S., and Navarra, A.: Bidimensional Diagnostics, Variability, and Trends of Northern
573 Hemisphere Blocking. J. Climate, 25, 6496-6509, doi:10.1175/JCLI-D-12-00032.1, 2012.
574 Dee, D. P., Uppala, S. M., Simmons, A. J., Berrisford, P., Poli, P., Kobayashi, S., Andrae, U., Balmaseda, M. A., Balsamo,
575 G., Bauer, P., Bechtold, P., Beljaars, A. C. M., Van de Berg, L., Bidlot, J., Bormann, N., Delsol, C., Dragani, R.,
576 Fuentes, M., Geer, A. J., Haimberger, L., Healy, S. B., Hersbach, H., Hólm, E. V., Isaksen, L., Kållberg, P., Köhler,
577 M., Matricardi, M., McNally, A. P., Monge-Sanz, B. M., Morcrette, J., Park, B., Peubey, C., de Rosnay, P., Tavolato,
578 C., Thépaut, J., and Vitart, F.: The ERA-Interim reanalysis: configuration and performance of the data assimilation
579 system. Q. J. Roy. Meteorol. Soc., 137, 553-597, doi:10.1002/qj.828, 2011.
580 Dole, R., Hoerling, M., Perlwitz, J., Eischeid, J., Pegion, P., Zhang, T., Quan, X., Xu, T., and Murray, D.: Was there a basis
581 for anticipating the 2010 Russian heat wave? Geophys. Res. Lett., 38, n/a, doi:10.1029/2010GL046582, 2011.
582 Dong, L., Mitra, C., Greer, S., and Burt, E.: The Dynamical Linkage of Atmospheric Blocking to Drought, Heatwave and
583 Urban Heat Island in Southeastern US: A Multi-Scale Case Study. Atmosphere, 9, 33, doi:10.3390/atmos9010033,
584 2018.
585 Dunn-Sigouin, E., Son, S.: Northern Hemisphere blocking frequency and duration in the CMIP5 models. J. Geophys. Res.-
586 Atmos. 118, 1179-1188, doi:10.1002/jgrd.50143, 2013.
587 E. K. M. Chang, Lee, S., and Swanson, K.L.: Storm Track Dynamics. J. Climate, 15, 2163-2183, doi:10.1175/1520-
588 0442(2002)015<02163:STD>2.0.CO;2, 2002.
589 Egger, J.: Dynamics of Blocking Highs. J. Atmos. Sci., 35, 1788-1801, doi:10.1175/1520-
590 0469(1978)035<1788:DOBH>2.0.CO;2, 1978.
591 Frierson, D. M. W.: The Dynamics of Idealized Convection Schemes and Their Effect on the Zonally Averaged Tropical
592 Circulation. J. Atmos. Sci., 64, 1959-1976, doi:10.1175/JAS3935.1, 2007.

Frierson, D. M. W., Held, I. M., and Zurita-Gotor, P.: A Gray-Radiation Aquaplanet Moist GCM. Part I: Static Stability and Eddy Scale. J. Atmos. Sci., 63, 2548-2566, doi:10.1175/JAS3753.1, 2006.

Frierson, D. M. W., Held, I. M., and Zurita-Gotor, P.: A Gray-Radiation Aquaplanet Moist GCM. Part II: Energy Transports in Altered Climates. J. Atmos. Sci., 64, 1680-1693, doi:10.1175/JAS3913.1, 2007.

Geen, R., Lambert, F. H. and Vallis, G. K.: Regime Change Behavior during Asian Monsoon Onset. J. Climate, 31, 3327-3348, doi:10.1175/JCLI-D-17-0118.1, 2018.

Grose, W. L., Hoskins, B. J.: On the Influence of Orography on Large-Scale Atmospheric Flow. J. Atmos. Sci., 36, 223-234, doi:10.1175/1520-0469(1979)036<0223:OTIOOO>2.0.CO;2, 1979.

Guo, Y., Chang, E. K. M., and Leroy, S. S.: How strong are the Southern Hemisphere storm tracks? Geophys. Res. Lett., 36, L22806, doi:10.1029/2009GL040733. 2009.

Hassanzadeh, P., Kuang, Z., and Farrell, B. F.: Responses of midlatitude blocks and wave amplitude to changes in the meridional temperature gradient in an idealized dry GCM. Geophys. Res. Lett., 41, 5223-5232, doi:10.1002/2014GL060764, 2014.

Held, I. M., Ting, M., and Wang, H.: Northern Winter Stationary Waves. J. Climate, 15, 2125-2144, doi:10.1175/1520-0442(2002)015<2125:NWSWTA>2.0.CO;2, 2002.

Hu, Y., Yang, D., and Yang, J.: Blocking systems over an aqua planet. Geophys. Res. Lett., 35, L19818-n/a, doi:10.1029/2008GL035351, 2008.

Hodges, K. I., Lee, R. W., and Bengtsson, L.: A Comparison of Extratropical Cyclones in Recent Reanalyses ERA-Interim, NASA MERRA, NCEP CFSR, and JRA-25. J. Climate, 24, 4888-4906, doi:10.1175/2011JCLI4097.1, 2011.

Luo, D.: A Barotropic Envelope Rossby Soliton Model for Block–Eddy Interaction. Part I: Effect of Topography. J. Atmos. Sci., 62, 5-21, doi:10.1175/1186.1, 2005.

Lutsko, N. J., Held, I. M.: The Response of an Idealized Atmosphere to Orographic Forcing: Zonal versus Meridional Propagation. J. Atmos. Sci., 73, 3701-3718, doi:10.1175/JAS-D-16-0021.1, 2016.

Croci-Maspoli, M., Schwierz, C., and Davies, H. C.: A Multifaceted Climatology of Atmospheric Blocking and Its Recent Linear Trend. J. Climate, 20, 633-649, doi:10.1175/JCLI4029.1, 2007.

Manabe, S., Terpstra, T. B.: The Effects of Mountains on the General Circulation of the Atmosphere as Identified by Numerical Experiments. J. Atmos. Sci., 31, 3-42, doi:10.1175/1520-0469(1974)031<0003:TEOMOT>2.0.CO;2, 1974.

Masato, G., Hoskins, B. J., and Woollings, T. J.: Wave-breaking characteristics of midlatitude blocking. Q. J. Roy. Meteorol. Soc., 138, 1285-1296, doi:10.1002/qj.990, 2012.

Matsueda, M., Mizuta, R. and Kusunoki, S.: Future change in wintertime atmospheric blocking simulated using a 20-km-mesh atmospheric global circulation model. J. Geophys. Res.-Atmos., 114, D12114-n/a, doi:10.1029/2009JD011919, 2009.

Mattingly, K. S., McLeod, J. T., Knox, J. A., Shepherd, J. M., and Mote, T. L.: A climatological assessment of Greenland blocking conditions associated with the track of Hurricane Sandy and historical North Atlantic hurricanes. International Journal of Climatology, 35, 746-760, doi:10.1002/joc.4018, 2015.

Nabizadeh, E., Hassanzadeh, P., Yang, D., and Barnes, E. A.: Size of the Atmospheric Blocking Events: Scaling Law and Response to Climate Change. Geophys. Res. Lett., 46, 13488-13499, doi:10.1029/2019GL084863, 2019.

Nakamura, H., Nakamura, M., and Anderson, J. L.: The Role of High- and Low-Frequency Dynamics in Blocking Formation. Mon. Weather Rev., 125, 2074-2093, doi:10.1175/1520-0493(1997)125<2074:TROHAL>2.0.CO;2, 1997.

Nakamura, H., Shimpo, A.: Seasonal Variations in the Southern Hemisphere Storm Tracks and Jet Streams as Revealed in a Reanalysis Dataset. J. Climate, 17, 1828-1844, doi:10.1175/1520-0442(2004)017<1828:SVITSH>2.0.CO;2, 2004.

Nakamura, N., Huang, C. S. Y.: Atmospheric blocking as a traffic jam in the jet stream. Science, 361, 42-47, doi:10.1126/science.aat0721, 2018.

O'Gorman, P. A., Schneider, T.: The Hydrological Cycle over a Wide Range of Climates Simulated with an Idealized GCM. J. Climate, 21, 3815-3832, doi:10.1175/2007JCLI2065.1, 2008.

Parsons, S., Renwick, J. A., and McDonald, A. J.: An Assessment of Future Southern Hemisphere Blocking Using CMIP5 Projections from Four GCMs. J. Climate, 29, 7599-7611, doi:10.1175/JCLI-D-15-0754.1, 2016.

Pelly, J. L., Hoskins, B. J.: A New Perspective on Blocking. J. Atmos. Sci., 60, 743-755, doi:10.1175/1520-0469(2003)060<0743:ANPOB>2.0.CO;2, 2003.

Pfahl, S., Schwierz, C., Croci-Maspoli, M., Grams, C. M., and Wernli, H.: Importance of latent heat release in ascending air streams for atmospheric blocking. Nat. Geosci., 8, 610-614, doi:10.1038/ngeo2487, 2015.

Pfahl, S., Wernli, H.: Quantifying the relevance of atmospheric blocking for co-located temperature extremes in the Northern Hemisphere on (sub-)daily time scales. Geophys. Res. Lett., 39, n/a, doi:10.1029/2012GL052261, 2012.

Pithan, F., Shepherd, T. G., Zappa, G., Sandu, I.: Climate model biases in jet streams, blocking and storm tracks resulting from missing orographic drag. Geophys. Res. Lett., 43, 7231-7240, doi:10.1002/2016GL069551, 2016.

Quintanar, A. I., Mechoso, C. R.: Quasi-Stationary Waves in the Southern Hemisphere. Part I: Observational Data. J. Climate, 8, 2659-2672, doi:10.1175/1520-0442(1995)008<2659:QSWITS>2.0.CO;2, 1995.

Renwick, J. A.: Persistent Positive Anomalies in the Southern Hemisphere Circulation. Mon. Weather Rev., 133, 977-988, doi:10.1175/MWR2900.1, 2005.

Rex, D. F.: Blocking Action in the Middle Troposphere and its Effect upon Regional Climate. Tellus, 2, 196-211, doi:10.3402/tellusa.v2i3.8546, 1950.

Sausen, R., König, W., and Sielmann, F.: Analysis of blocking events from observations and ECHAM model simulations. Tellus A, 47, 421-438, doi:10.3402/tellusa.v47i4.11526, 1995.

Shutts, G. J.: The propagation of eddies in diffluent jetstreams: Eddy vorticity forcing of 'blocking' flow fields. Q. J. Roy. Meteorol. Soc., 109, 737-761, doi:10.1002/qj.49710946204, 1983

Sillmann, J., Croci-Maspoli, M., Kallache, M., and Katz, R. W.: Extreme Cold Winter Temperatures in Europe under the Influence of North Atlantic Atmospheric Blocking. J. Climate, 24, 5899-5913, doi:10.1175/2011JCLI4075.1, 2011.

Strong, C., Magnusdottir, G.: Tropospheric Rossby Wave Breaking and the NAO/NAM. J. Atmos. Sci., 65, 2861-2876, doi:10.1175/2008JAS2632.1, 2008.

Takaya, K., Nakamura, H.: A Formulation of a Phase-Independent Wave-Activity Flux for Stationary and Migratory Quasigeostrophic Eddies on a Zonally Varying Basic Flow. J. Atmos. Sci., 58, 608-627, doi:10.1175/1520-0469(2001)058<0608:AFOAPI>2.0.CO;2, 2001.

Trenberth, K. E.: Storm Tracks in the Southern Hemisphere. J. Atmos. Sci., 48, 2159-2178, doi:10.1175/1520-0469(1991)048<2159:STITSH>2.0.CO;2, 1991.

Troen, I. B., Mahrt, L.: A simple model of the atmospheric boundary layer; sensitivity to surface evaporation. Bound.-Lay. Meteorol., 37, 129-148, doi:10.1007/BF00122760, 1986.

Tung, K. K., Lindzen, R. S.: A Theory of Stationary Long Waves. Part I: A Simple Theory of Blocking. Mon. Weather Rev., 107, 714-734, doi:10.1175/1520-0493(1979)107<0714:ATOSLW>2.0.CO;2, 1979.

Valdes, P. J., Hoskins, B. J.: Nonlinear Orographically Forced Planetary Waves. J. Atmos. Sci., 48, 2089-2106, doi:10.1175/1520-0469(1991)048<2089:NOFPW>2.0.CO;2, 1991.

Vallis, G. K., Colyer, G., Geen, R., Gerber, E., Jucker, M., Maher, P., Paterson, A., Pietschnig, M., Penn, J., and Thomson, S. I.: Isca, v1.0: a framework for the global modelling of the atmospheres of Earth and other planets at varying levels of complexity. Geosci. Model Dev., 11, 843-859, doi:10.5194/gmd-11-843-2018, 2018.

Wallace, J. M., Lim, G., and Blackmon, M. L.: Relationship between Cyclone Tracks, Anticyclone Tracks and Baroclinic Waveguides. J. Atmos. Sci., 45, 439-462, doi:10.1175/1520-0469(1988)045<0439:RBCTAT>2.0.CO;2, 1988.

Wang, L., Z. Kuang, Z.: Evidence against a general positive eddy feedback in atmospheric blocking. arXiv preprint arXiv:1907.00999. 2019

White, R. H., Battisti, D. S., and Roe, G. H.: Mongolian Mountains Matter Most: Impacts of the Latitude and Height of Asian Orography on Pacific Wintertime Atmospheric Circulation. J. Climate, 30, 4065-4082, doi:10.1175/JCLI-D-16-0401.1, 2017.

Wirth, V., Riemer, M., Chang, E. K. M., and Martius, O.: Rossby Wave Packets on the Midlatitude Waveguide—A Review. Mon. Weather Rev., 146, 1965-2001, doi:10.1175/MWR-D-16-0483.1, 2018.

Woollings, T., Barriopedro, D., Methven, J., Son, S., Martius, O., Harvey, B., Sillmann, J., Lupo, A., Seneviratne, S.: Blocking and its Response to Climate Change. Curr Clim Change Rep, 4, 287-300, doi:10.1007/s40641-018-0108-z, 2018.

Yamazaki, A., Itoh, H.: Vortex–Vortex Interactions for the Maintenance of Blocking. Part I: The Selective Absorption Mechanism and a Case Study. J. Atmos. Sci., 70, 725-742, doi:10.1175/JAS-D-11-0295.1, 2013.

Configuration	Region	Western Edge	Eastern Edge
Single Mountain (SingleMtn)	East	0˚	90˚ E
	Other	90˚ E	0˚
Two Mountains (TwoMtn)	Wide Basin East	0˚	90˚ E
	Wide Basin Other	150˚ W	0˚
	Short Basin	90˚ E	150˚ W

689 **Table 1: Regions used for subsetting blocks in the compositing and duration analysis. Each region spans 30˚- 65˚ N, for the longitudes**
690 **listed in the table.**

691

Configuration	Area Averaged Block Frequency (%), 30° N- 90° N	Number of Events
Aquaplanet	**3.24**	**387**
1 km single mountain	**3.17**	**365**
2 km single mountain	**3.67**	**400**
3 km single mountain	**3.74**	**438**
4 km single mountain	**3.84**	**433**
Two 3 km mountains (TwoMtn)	**4.01**	**423**

692 **Table 2: Cool season area-averaged block frequency and number of events in the idealized model integrations.**

693

	Mean block duration (days) and number of events			
	All Midlatitude Blocks	East blocks		Other blocks
Aquaplanet	7.53 (227)	-		-
1 km mountain	7.78 (206)	8.65 (58)		7.44 (148)
2 km mountain	7.93 (234)	8.54 (75)		7.64 (159)
3 km mountain	7.55 (266)	7.91 (103)		7.31 (163)
4 km mountain	7.78 (244)	7.99 (81)		7.68 (163)
Two 3 km mountains (TwoMtn)	8.17 (238)	Wide Basin	8.35 (81)	8.47 (86)
		Short Basin	7.65 (68)	

694 **Table 3: Mean block duration and number of events in parentheses for midlatitude, cool season blocks in each idealized model**
695 **configuration.**

696

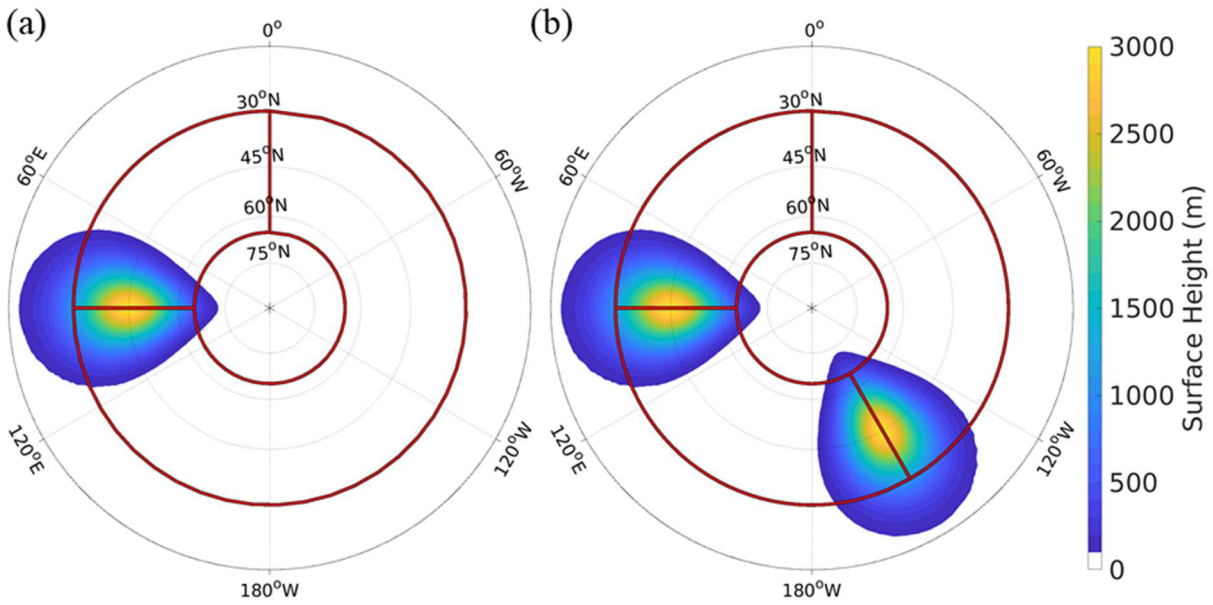

Figure 1: Surface height (shading) of the idealized model integrations with (a) a single 3 km high Gaussian mountain centered at 45 N, 90E and (b) two 3 km high Gaussian mountains centered at 45 N, 90E and 45 N, 150 W, respectively. The red outlines indicate the block genesis regions described in Table 1.

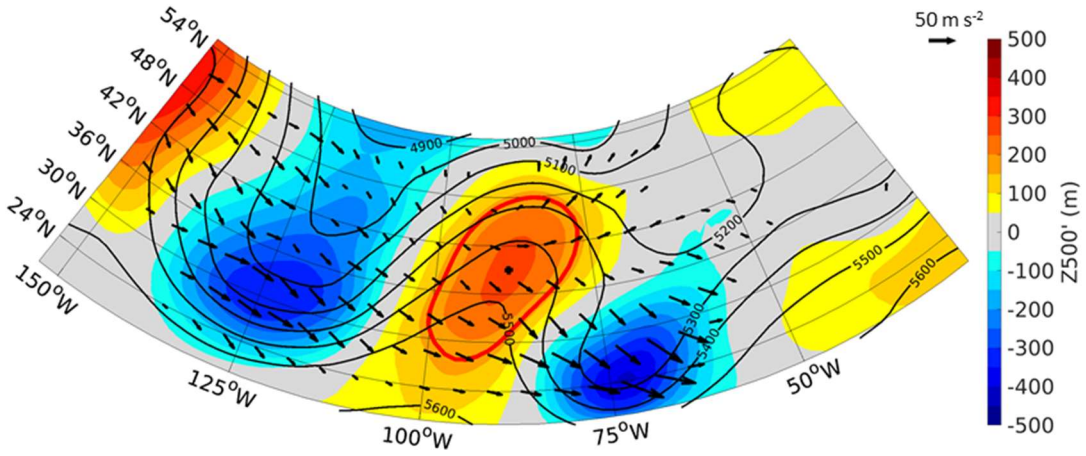

Figure 2: 500 hPa geopotential height (black contours), 500 hPa geopotential height anomaly (shading), outline of blocked area (red contour), and wave activity flux vectors $\vec{W}$ (black arrows), for the first day of a blocking episode in the aquaplanet run. The black dot inside the block denotes the block centroid. Geopotential height contours are in 100 m intervals. $\vec{W}$ with magnitudes less than 20 m^2 s^{-2} are removed.

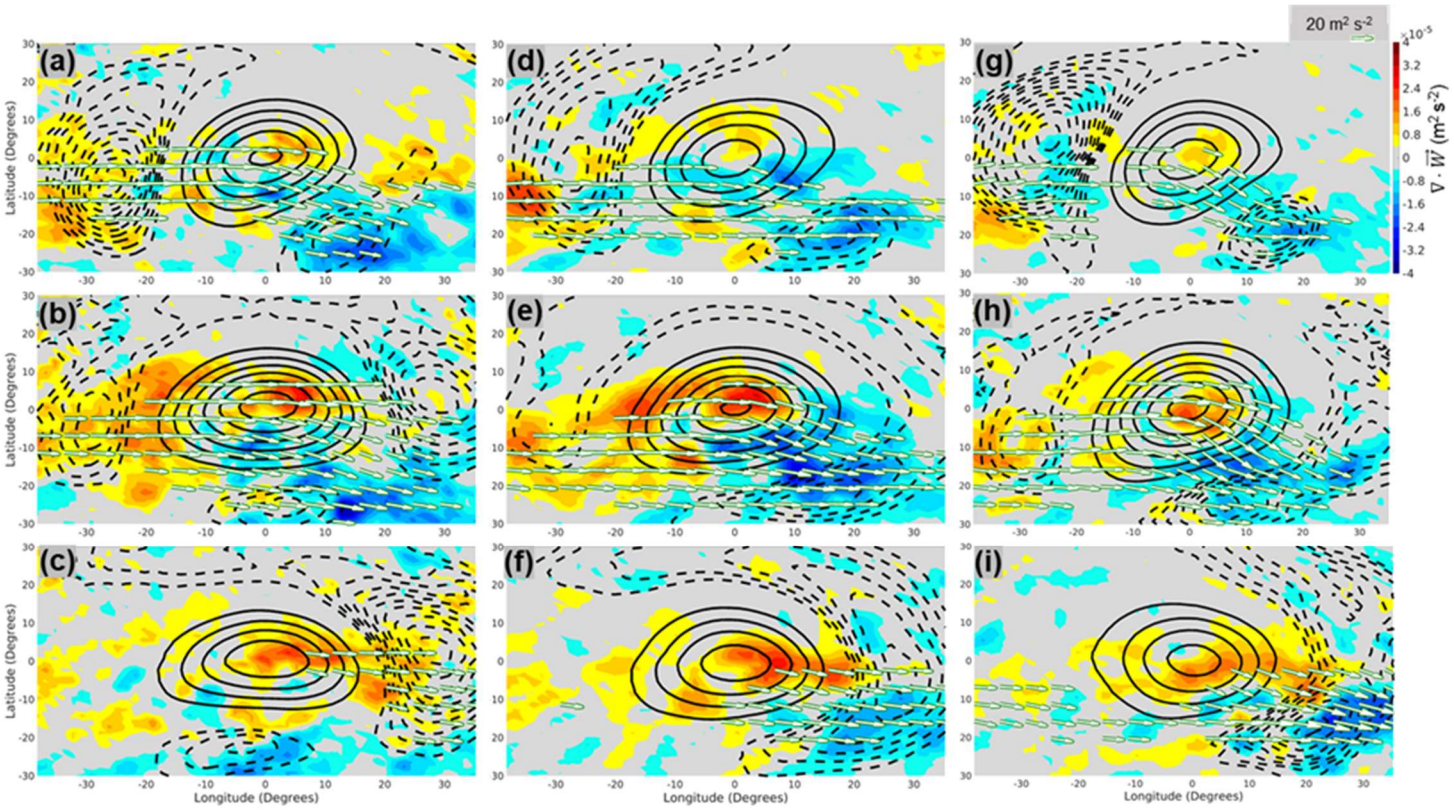

Figure 3: For cool season blocking events: Block centered composites of positive 500 hPa geopotential height anomalies (solid contours), negative 500 hPa geopotential height anomalies (dotted contours), $\vec{W}$ (arrows), and $\nabla \cdot \vec{W}$ (shading). (a-c) Left: Computed with SH blocks in ERA-Interim. (d-f) Centre: Computed with blocks in the aquaplanet integration. (g-i) Right: Computed with blocks in the 3 km single mountain integration. The top, middle, and bottom rows are composites over the first, strongest, and last timesteps of blocking episodes, respectively. Positive (negative) 500 hPa geopotential height anomaly contours are in 50 m (-10 m) intervals with outer contour 50 m (-30 m). $\vec{W}$ with magnitudes less than 20 m^2 s^{-2} are removed. Latitude and longitude are defined relative to the composite block center.

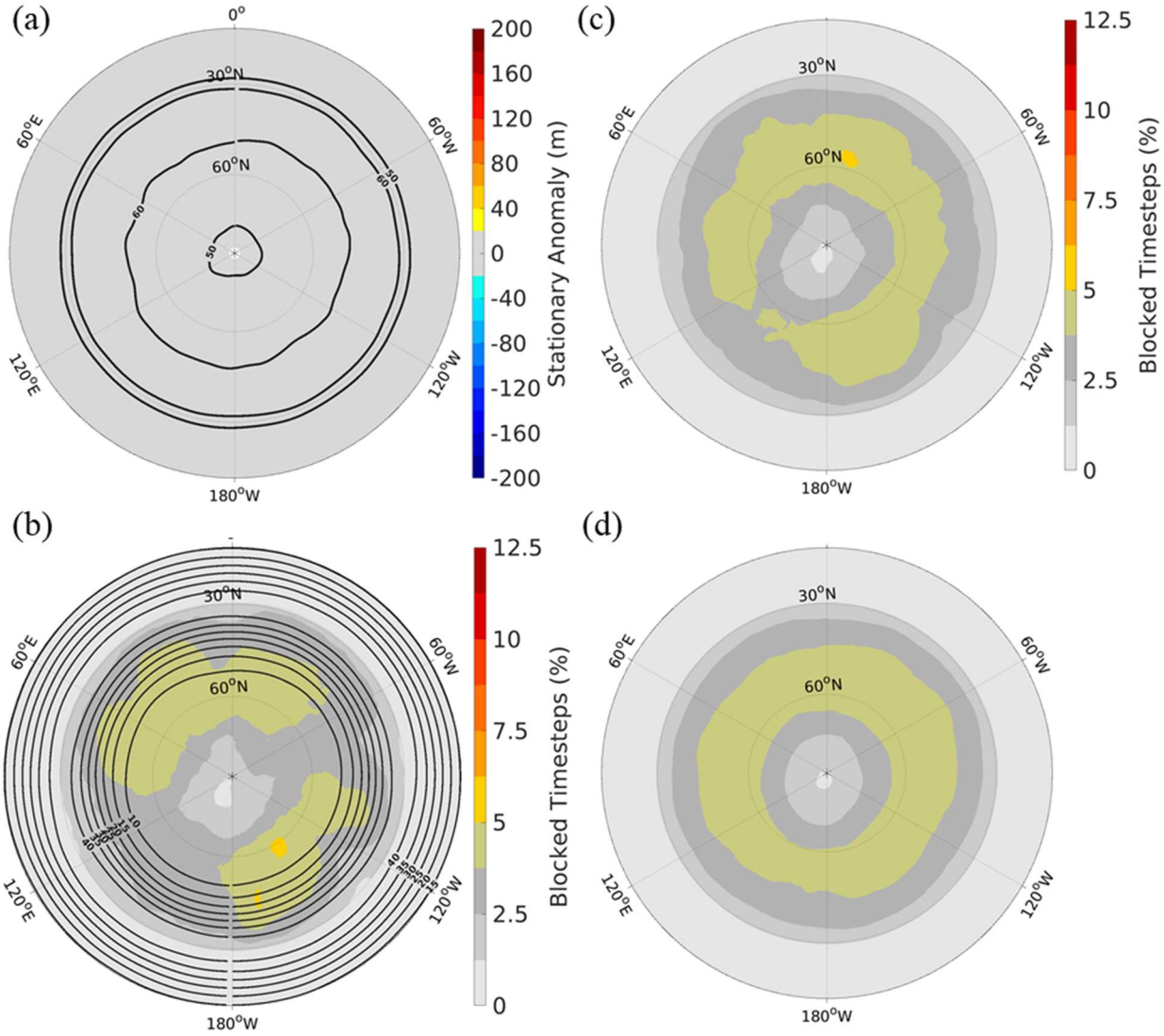

Figure 4: (a and c) Top: For 30 cool seasons (Nov.-Mar.) in the aquaplanet, (a) the stationary wave (shading) and storm track (heavy black contours), and (c) the blocking climatology (shading) and $\overline{U250}$ (heavy black contours) for the idealized model aquaplanet integration. (b and d) Bottom: Blocking climatology (shading) for (c) 100 and (d) 250 cool seasons in the aquaplanet. In (a) storm track contours are in 10 m intervals where the outer contour is 50 m. In (c) $\overline{U250}$ contours are in 5 m/s intervals where the outer contour is 30 m s^{-1}

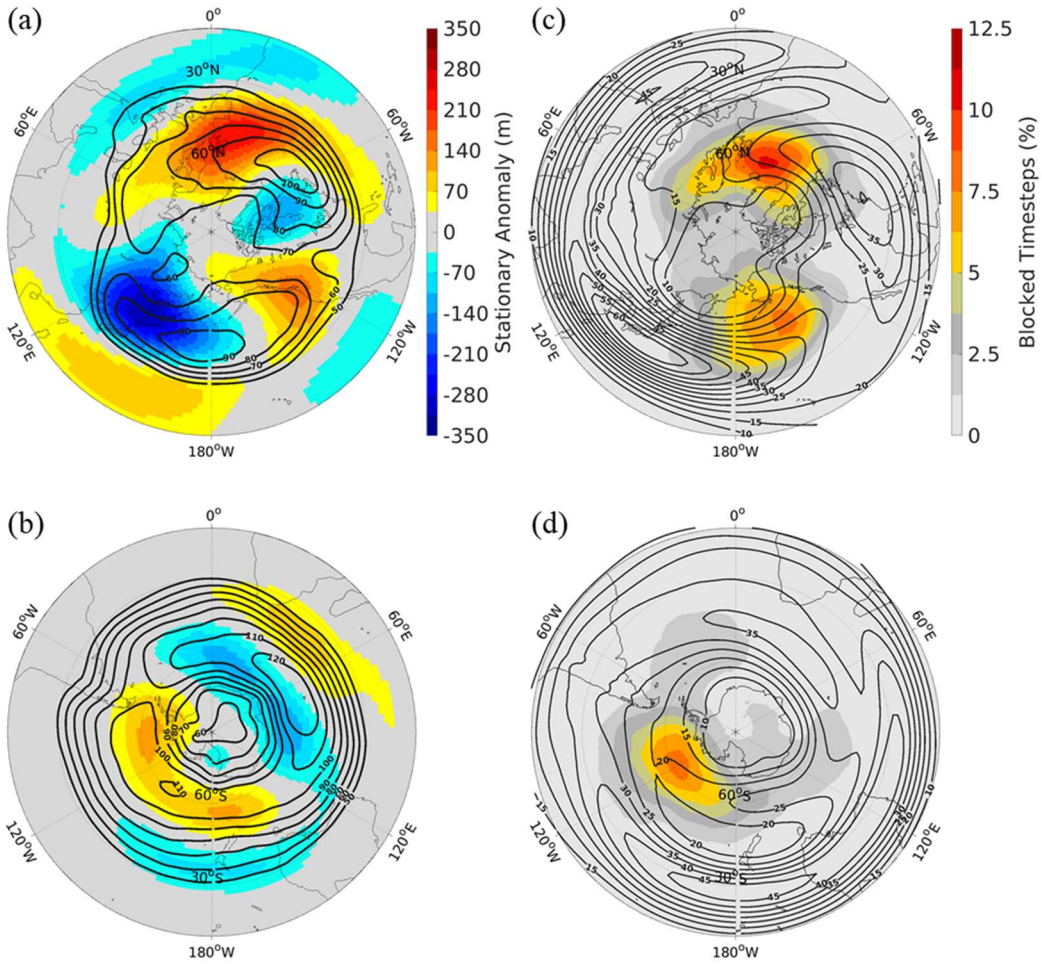

724

725 **Figure 5: (a-b) Left: Cool season stationary wave (shading) and storm track (heavy black contours) for the (a) northern and (b)**
726 **southern hemispheres in ERA-Interim. Storm track contours are in 10 m intervals where the outer contour is 50 m. (c-d) Right:**
727 **Cool season blocking climatology (shading) and $\overline{U250}$ (heavy black contours) for the (c) northern and (d) southern hemispheres in**
728 **ERA-Interim. $\overline{U250}$ contours are in 5 m/s intervals where the outer contour is 10 m s^{-1}.**

729

730

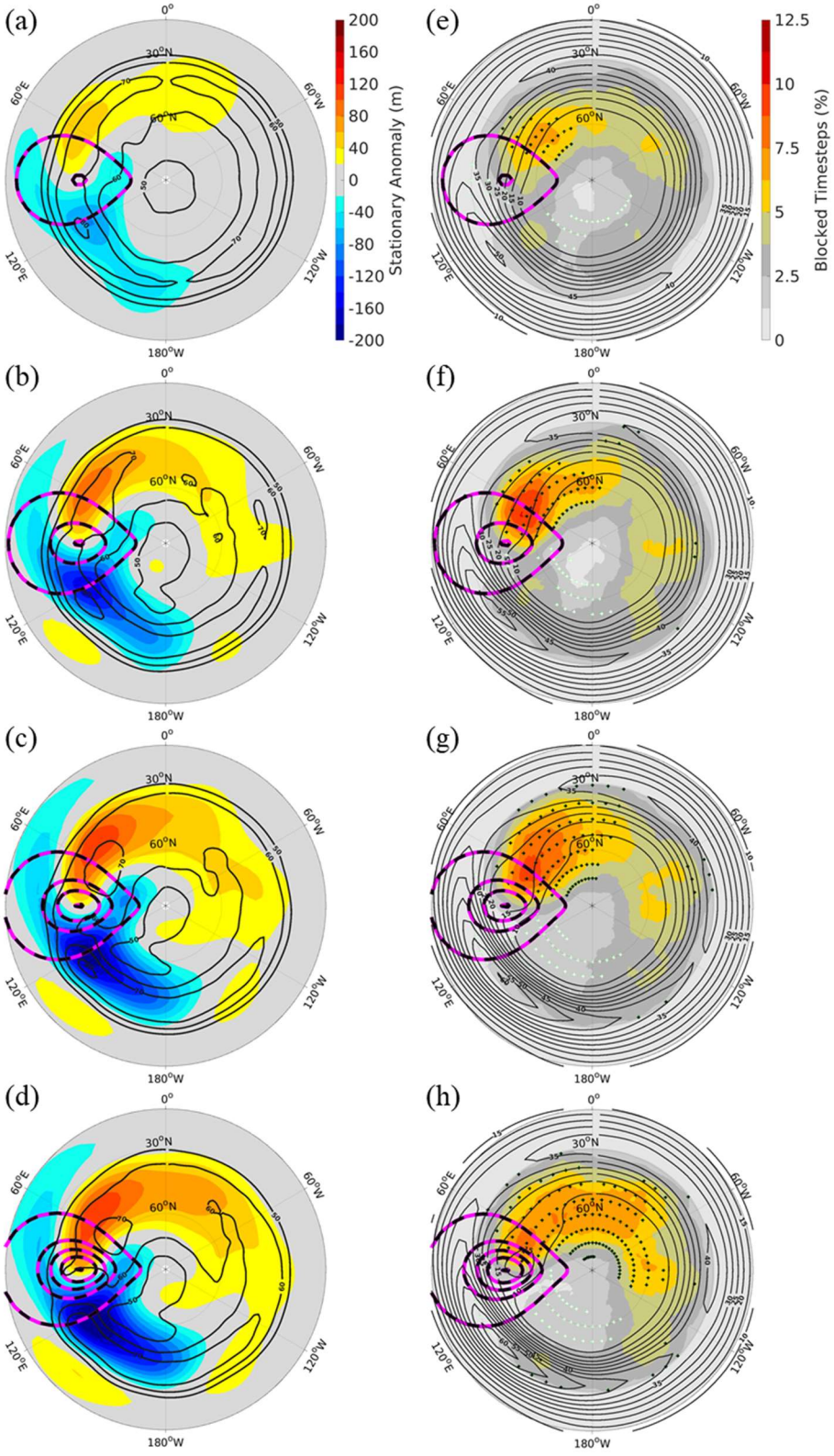
(a)
(b)
(c)
(d)
(e)
(f)
(g)
(h)
Stationary Anomaly (m)
200
160
120
80
40
0
-40
-80
-120
-160
-200
Blocked Timesteps (%)
12.5
10
7.5
5
2.5
0
0°
30°N
60°N
60°E
60°W
120°E
120°W
180°W

Figure 6: (a-d) Left: Cool season stationary wave (shading) and storm track (heavy black contours) for the (a) 1 km, (b) 2 km, (c) 3 km, and (d) 4 km mountain height integrations. Storm track contours are in 10 m intervals where the outer contour is 50 m. (e-h) Right: Cool season blocking climatology (shading) and $\overline{U250}$ (heavy black contours) for the (e) 1 km, (f) 2 km, (g) 3 km, and (h) 4 km mountain height integrations. $\overline{U250}$ contours are in 5 m/s intervals where the outer contour is 10 m s^{-1}. Black (white) stippling in (e-h) indicates significantly greater (less) block frequency at nearby gridpoints when compared to a 250-year aquaplanet integration. Pink and black dotted contours represent surface height, where the outer contour is the edge of the land-mask and the inner contours are in 1 km intervals.

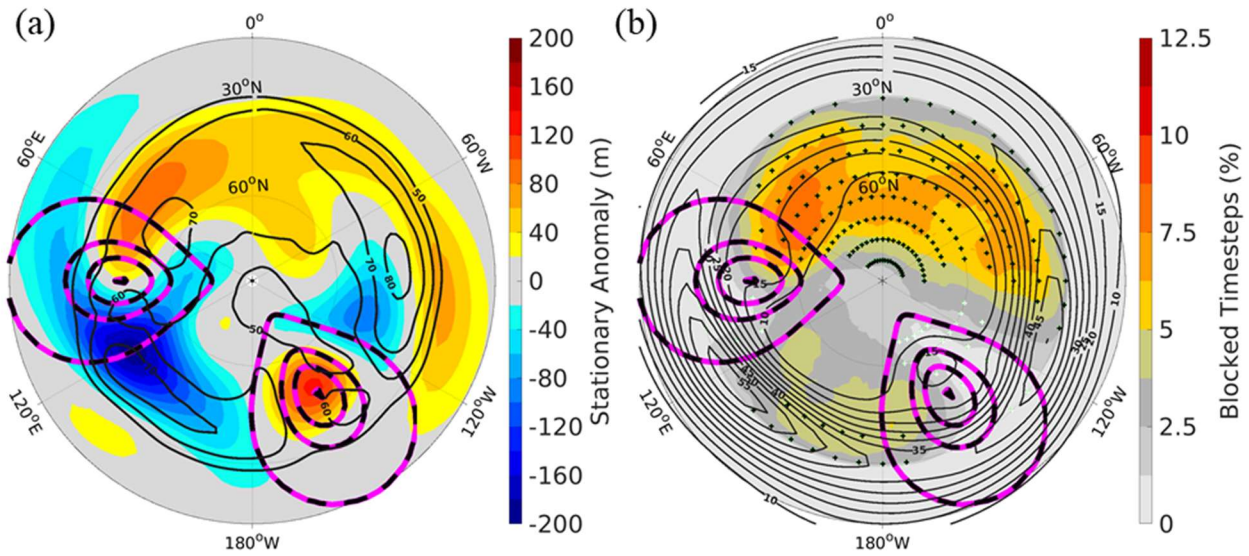

Figure 7: For the 2-mountain idealized model integration, (a) the cool season stationary wave (shading) and storm track (heavy black contours), and (b) the cool season blocking climatology (shading) and $\overline{U250}$ (heavy black contours). In (a) storm track contours are in 10 m intervals where the outer contour is 50 m. In (b) $\overline{U250}$ contours are in 5 m/s intervals where the outer contour is 10 m s^{-1}. Black (white) stippling in b indicates significantly greater (less) block frequency at nearby gridpoints when compared to a 250-year aquaplanet integration. Pink and black dotted contours represent surface height, where the outer contour is the edge of the land-mask and the inner contours are in 1 km intervals.

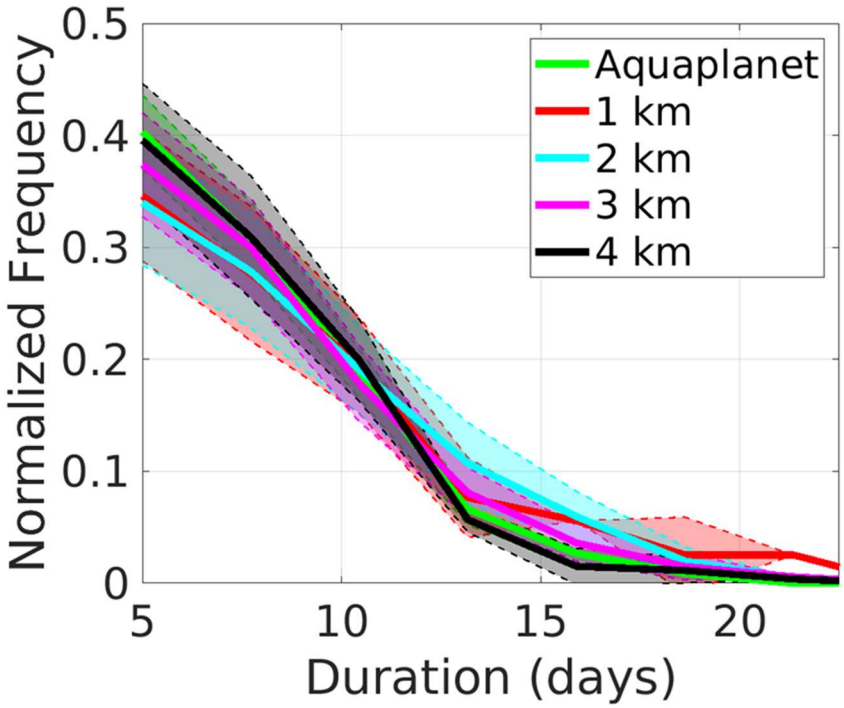

Figure 8: Block duration probability density distributions for the aquaplanet and "East" blocks (as defined in table 1) in the single mountain configurations. Thick lines denote the mean probability density distribution for each configuration. Shaded regions bordered by dotted lines outline +/- 1 full standard deviation from the mean.

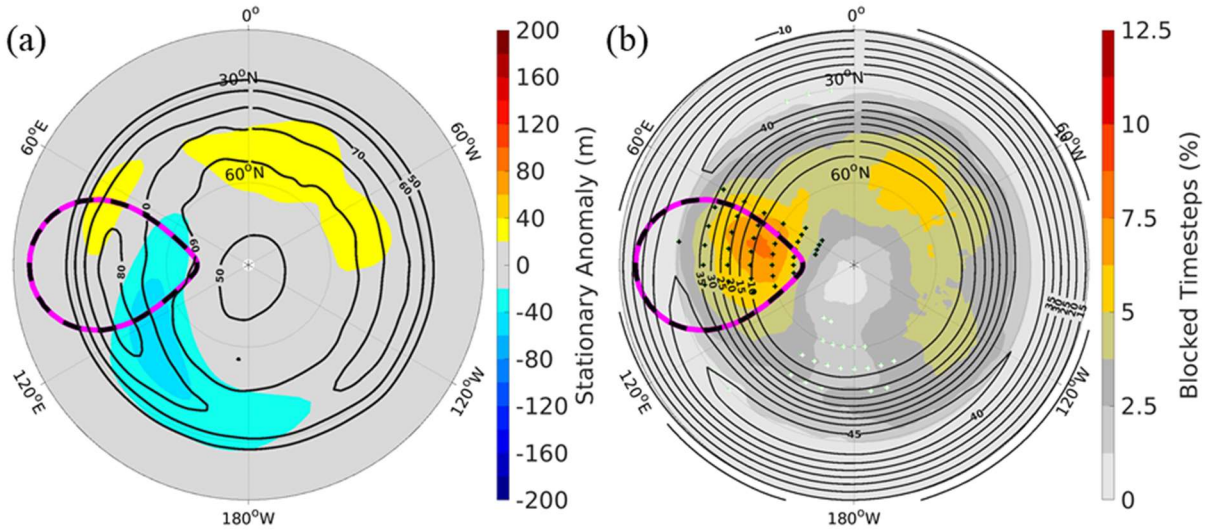

753

754 **Figure 9: For an integration with 1 flat landmass, (a) the cool season stationary wave (shading) and storm track (heavy black**
755 **contours), and (b) the cool season blocking climatology (shading) and $\overline{U250}$ (heavy black contours). In (a) storm track contours are**
756 **in 10 m intervals where the outer contour is 50 m. In (b) $\overline{U250}$ contours are in 5 m/s intervals where the outer contour is 10 m s^{-1}.**
757 **Black (white) stippling in b indicates significantly greater (less) block frequency at nearby gridpoints when compared to a 250-year**
758 **aquaplanet integration. The pink and black dotted contours represent the outer edge of the land-mask.**